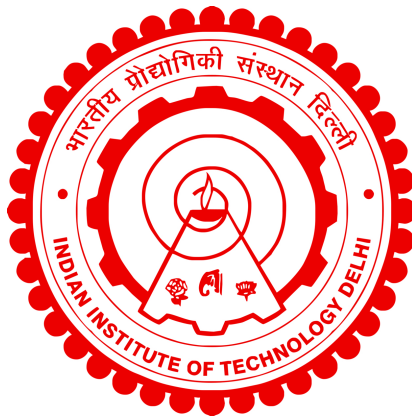


**COMPREHENSIVE ANALYSIS OF THE
D₂-LINE SPECTROSCOPIC FEATURES IN
THERMAL RUBIDIUM VAPOR**

RAJNI BALA



DEPARTMENT OF PHYSICS

**INDIAN INSTITUTE OF TECHNOLOGY DELHI
NEW DELHI-110016
OCTOBER 2024**

© Indian Institute of Technology Delhi (IITD), New Delhi, 2024

**COMPREHENSIVE ANALYSIS OF THE
D₂-LINE SPECTROSCOPIC FEATURES IN
THERMAL RUBIDIUM VAPOR**

by

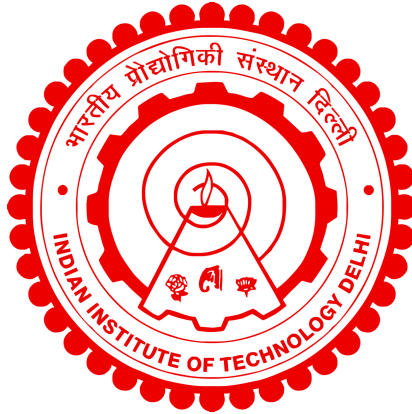
Rajni Bala

Department of Physics

Submitted

in partial fulfillment of the requirements of the degree of Doctor of Philosophy

to the



**INDIAN INSTITUTE OF TECHNOLOGY
DELHI
OCTOBER 2024**

Dedicated to my loving parents

Certificate

This is to certify that the thesis entitled “**COMPREHENSIVE ANALYSIS OF THE D₂-LINE SPECTROSCOPIC FEATURES IN THERMAL RUBIDIUM VAPOR**”, submitted by **Rajni Bala** to the Indian Institute of Technology Delhi, for the award of the degree of **Doctor of Philosophy** in Physics, is a record of the original, bonafide research work carried out by her under my supervision and guidance. The thesis has reached standards that meet the requirements of the regulations related to the award of the degree.

The results in this thesis have not been submitted in part or in whole to any other University or Institute for awarding any degree or diploma to the best of our knowledge.

Prof. Vivek Venkataraman

Department of Electrical Engineering

Joint appointment with the Department of Physics

Indian Institute of Technology Delhi.

Acknowledgements

I extend my sincere gratitude to my supervisor, Prof. Vivek Venkataraman, for his unwavering guidance, encouragement, and invaluable insight throughout the research process. This work has greatly benefited from his support, patience, and perceptive criticism.

Additionally, I am grateful to my SRC committee members, Prof. Siddharth Pandey, Prof. Joyee Ghosh, and Prof. Sunil Kumar, for their insightful comments, generous allocation of time, and helpful feedback, all of which have significantly improved the quality of this thesis.

I would like to express my heartfelt thanks to my seniors, Dr. Ramesh Kumar, Dr. Vineet Kumar Shukla, and Dr. Shivani Sharma, for their valuable discussions and encouragement. I appreciate Omshanker, my research companion and dear friend, for his support, positivity, friendship, and enthusiasm. His excitement about the topic has always served as an inspiration. Special thanks go to Dr. Vaishnavi Rajagopal for her continuous efforts to improve my presentation and research writing skills.

I also extend my thanks to my juniors, Vikash, Bharti, Kaustav, Vijay, and Akanksha, for their infectious energy and fresh perspectives. Their willingness to learn and grow has positively impacted our collective success.

I am grateful to the academic and technical staff of IIT Delhi for their assistance in providing access to research facilities, resources, and administrative support. I also acknowledge the financial support provided by CSIR, which enabled me to carry out this research and pursue my academic goals.

I am deeply indebted to my family for their constant support, love, and understanding. My optimistic outlook has been shaped by the unconditional affection and encouragement of my parents, Rohit Bhaiya, Priya Bhabhi, Vipin Bhaiya, Mohit Bhaiya, and my niece Jagriti. Their belief in me and their support have been my greatest motivation. I appreciate my friend and spouse, Ajay, for always being there for me, listening to my problems, and helping me navigate both the good and bad times. Additionally, I thank my wonderful friends Om, Nisha, and Komal for their

support. Their kindness and presence have profoundly influenced my journey, for which I am truly grateful.

I genuinely thank everyone who has contributed to making this thesis a reality, regardless of the size of their contribution.

Thank you, Almighty.

Rajni Bala

Abstract

Alkali atoms are ideal candidates for high-resolution spectroscopy owing to their ability to strongly interact with visible and near-infrared (NIR) light, where tunable high-power lasers with narrow linewidths ($\lesssim 100$ kHz, much smaller than their natural linewidth, ~ 10 MHz, for the strongest D-line transitions) are commercially available. Due to their structural simplicity similar to the H-atom along with a large vapor atomic density ($\sim 10^{16}$ atoms/m³ even at near-room temperature), alkalis provide an easily addressable system to probe various phenomena such as Doppler-broadening, two-level saturation, optical-pumping-induced birefringence in a closed system, absorption saturation in an open system, etc. The alkali D-line transitions (having open and closed atomic transitions) have a wide range of applications in the classical as well as quantum domain, e.g., in Doppler-free spectroscopy, four-wave mixing, laser frequency stabilization, atomic clocks, cold atoms, slowing and storing light, quantum memories, etc. This thesis is a comprehensive theoretical and experimental investigation of some of these important classical atom-optical interactions. We provide simpler, less resource-intensive, efficient yet accurate computational models for these interactions, and experimentally validate their predictions without using any fitting parameters.

The most straightforward yet useful probes of the D-line transitions in alkali atoms are the Doppler-broadened and Doppler-free spectroscopies. These techniques require minimal experimental setups and are helpful in practically determining/calibrating fundamental atomic constants such as saturation intensity, vapor atomic density, energy level spacing, etc. The primary focus of this thesis is the Rb D₂-line comprising strong electric-dipole hyperfine transitions with large oscillator strength (~ 0.7), precisely determined transition probabilities, and long coherence time of the hyperfine ground states. We present *ab-initio* reduced rate equation models with a maximum of 7 levels to predict the effects of optical pumping, including hyperfine and Zeeman, transit relaxation, two-level saturation, etc., on the Doppler-broadened and Doppler-free absorption features of an alkali vapor system. We also experimentally validate our models for the Rb D₂-line transitions without any fitting parameters, and therefore show that they can be readily extended to other atomic systems. Furthermore, these simpler models require $\sim 100\times$ less memory/space

than the full multi-level models that comprise all (minimum 17) magnetic sub-levels of the Rb D₂-line hyperfine transitions.

Finally, this thesis also thoroughly explores Polarization Spectroscopy (PS), a Doppler-free spectroscopic technique, for laser frequency stabilization. We provide an extensive experimental investigation of the error signal generated directly via PS for the Rb D₂-line transitions, including the examination of various external parameters that affect the PS signal, such as temperature of the vapor cell, beam diameter, and pump-probe intensities. Our study provides crucial insight into the limitations and applicability of existing multi-level models that are utilized to analyze and characterize the PS signal.

सार

क्षार परमाणु उच्च-रिजॉल्यूशन स्पेक्ट्रोस्कोपी के लिए आदर्श उम्मीदवार हैं, क्योंकि उनमें दृश्य और निकट-अवरक्त (NIR) प्रकाश के साथ दृढ़ता से अंतःक्रिया करने की क्षमता होती है, जहां संकीर्ण लाइनविड्थ ($\lesssim 100$ kHz, जो कि उनकी प्राकृतिक लाइनविड्थ, ~ 10 MHz, से बहुत छोटी है, जो कि सबसे मजबूत D-लाइन संक्रमण के लिए है) के साथ ट्यूनेबल उच्च-शक्ति लेजर व्यावसायिक रूप से उपलब्ध हैं। H-परमाणु के समान उनकी संरचनात्मक सरलता के कारण, साथ ही एक बड़े वाष्प परमाणु घनत्व ($\sim 10^{16}$ परमाणु/m³ कमरे के तापमान पर भी), क्षार विभिन्न घटनाओं जैसे कि डॉपलर-ब्रॉडिंग, दो-स्तरीय संतृप्ति, एक बंद प्रणाली में ऑप्टिकल-पंपिंग-प्रेरित द्विभाजन, एक खुली प्रणाली में अवशोषण संतृप्ति आदि की जांच करने के लिए एक आसानी से संबोधित करने योग्य प्रणाली प्रदान करते हैं। क्षार D-लाइन संक्रमण (खुले और बंद परमाणु संक्रमण वाले) में शास्त्रीय और साथ ही क्वांटम डोमेन में अनुप्रयोगों की एक विस्तृत श्रृंखला है, उदाहरण के लिए, डॉपलर-मुक्त स्पेक्ट्रोस्कोपी, चार-तरंग मिश्रण, लेजर आवृत्ति स्थिरीकरण, परमाणु घड़ियां, ठंडे परमाणु, प्रकाश को धीमा करना और संग्रहीत करना, क्वांटम मेमोरी आदि। यह थीसिस इन महत्वपूर्ण शास्त्रीय परमाणु-ऑप्टिकल इंटरैक्शन में से कुछ की एक व्यापक सैद्धांतिक और प्रयोगात्मक जांच है। हम इन इंटरैक्शन के लिए सरल, कम संसाधन-गहन, कुशल लेकिन सटीक कम्प्यूटेशनल मॉडल प्रदान करते हैं, और किसी भी फिटिंग पैरामीटर का उपयोग किए बिना प्रयोगात्मक रूप से उनकी भविष्यवाणियों को मान्य करते हैं।

क्षार परमाणुओं में D-लाइन संक्रमण की सबसे सरल लेकिन उपयोगी जांच डॉपलर-विस्तृत और डॉपलर-मुक्त स्पेक्ट्रोस्कोपी हैं। इन तकनीकों के लिए न्यूनतम प्रयोगात्मक सेटअप की आवश्यकता होती है और ये संतृप्ति तीव्रता, वाष्प परमाणु घनत्व, ऊर्जा स्तर अंतर आदि जैसे मौलिक परमाणु स्थिरांक को व्यावहारिक रूप से निर्धारित/कैलिब्रेट करने में सहायक होते हैं। इस थीसिस का प्राथमिक फोकस Rb D₂-लाइन है जिसमें बड़ी ऑसिलेटर ताकत (~ 0.7), सटीक रूप से निर्धारित संक्रमण संभावनाओं और हाइपरफाइन ग्राउंड अवस्थाओं के लंबे सुसंगति समय के साथ मजबूत इलेक्ट्रिक-द्विध्रुवीय हाइपरफाइन संक्रमण शामिल हैं। हम हाइपरफाइन और ज़ीमैन, ट्रांजिट रिलैक्सेशन, दो-स्तरीय संतृप्ति आदि सहित ऑप्टिकल पंपिंग के प्रभावों की भविष्यवाणी करने के लिए अधिकतम 7 स्तरों के साथ ab-initio कम दर समीकरण मॉडल प्रस्तुत करते हैं, जो क्षार वाष्प प्रणाली की डॉपलर-विस्तृत और डॉपलर-मुक्त अवशोषण विशेषताओं पर होता है। हम बिना किसी फिटिंग पैरामीटर के Rb D₂-लाइन संक्रमणों के लिए अपने मॉडलों को प्रयोगात्मक रूप से मान्य करते हैं, और इसलिए दिखाते हैं कि उन्हें अन्य परमाणु प्रणालियों में आसानी से बढ़ाया जा सकता है। इसके अलावा, इन सरल मॉडलों को पूर्ण बहु-स्तरीय मॉडलों की तुलना में $\sim 100\times$ कम मेमोरी/स्पेस की आवश्यकता होती है, जिसमें Rb D₂-लाइन हाइपरफाइन संक्रमणों के सभी (न्यूनतम 17) चुंबकीय उप-स्तर शामिल होते हैं।

अंत में, यह थीसिस लेजर आवृत्ति स्थिरीकरण के लिए ध्रुवीकरण स्पेक्ट्रोस्कोपी (PS), एक डॉपलर-मुक्त स्पेक्ट्रोस्कोपिक तकनीक का भी गहन अन्वेषण करती है। हम Rb D₂-लाइन संक्रमणों के लिए PS के माध्यम से सीधे उत्पन्न त्रुटि संकेत की एक व्यापक प्रयोगात्मक जांच प्रदान करते हैं, जिसमें PS सिग्नल को प्रभावित करने वाले विभिन्न बाहरी मापदंडों की जांच

शामिल है, जैसे वाष्प सेल का तापमान, बीम व्यास और पंप-जांच तीव्रता। हमारा अध्ययन मौजूदा बहु-स्तरीय मॉडलों की सीमाओं और प्रयोज्यता के बारे में महत्वपूर्ण जानकारी प्रदान करता है जिनका उपयोग PS सिग्नल का विश्लेषण और विशेषता निर्धारण करने के लिए किया जाता है।

Contents

Certificate

Acknowledgements

Abstract

Contents

List of Figures

List of Tables

Abbreviations

Symbols

1	Introduction	1
1.1	Light-matter interaction	1
1.2	Quantum, semi-classical and classical treatments of atom-light interaction	2
1.3	Einstein rate equation model	7
1.3.1	Two-level system: closed system	8
1.3.2	Three-level system: open system	12
1.4	Characteristics of atomic spectroscopy	13
1.4.1	Fine and hyperfine spectra	13
1.4.2	Electric-dipole selection rules	15
1.4.3	Transition probability, line and oscillator strength	16
1.4.4	Spectral linewidth broadening mechanisms	18
1.4.5	Spectroscopic studies in thermal Rb vapor	24
1.5	Thesis Organisation	27

1.5.1	Chapter 2: A comprehensive model for Doppler spectra in thermal atomic vapor	28
1.5.2	Chapter 3: Competition between Zeeman and hyperfine pumping in thermal atomic vapor	28
1.5.3	Chapter 4: Impact of Zeeman sub-level pumping on saturated absorption spectra of thermal atomic vapor	29
1.5.4	Chapter 5: Optimization of Polarization Spectroscopy signal for laser frequency stabilization	30
1.5.5	Chapter 6: Conclusions and future directions	31
2	A comprehensive model for Doppler spectra in thermal atomic vapor	33
2.1	Introduction	34
2.2	Theory and calculations	37
2.2.1	5-level rate equation model for Rb D ₂ -line	38
2.2.2	Atomic population relaxation	40
2.2.2.1	Spontaneous decay rate:	40
2.2.2.2	Transit-relaxation rate:	41
2.2.3	Calculation of absorption coefficient	42
2.3	Experimental setup	44
2.4	Results and discussion	45
2.4.1	Effect of hyperfine pumping	45
2.4.2	Probe absorption as a function of beam diameter	47
2.4.3	Probe absorption as a function of vapor temperature	50
2.5	Conclusion	52
3	Competition between Zeeman and hyperfine pumping in thermal atomic vapor	57
3.1	Introduction	58
3.2	Theory and calculations	61
3.2.1	Atomic population relaxation	64
3.2.1.1	Spontaneous decay rate:	64
3.2.1.2	Transit-relaxation rate:	66
3.2.2	Calculation of absorption coefficient	68
3.3	Experimental setup	68
3.4	Results and discussion	69
3.4.1	Probe absorption as a function of its polarization	71
3.4.2	Interplay between Zeeman and hyperfine pumping	73
3.5	Conclusions	75
4	Impact of Zeeman sub-level pumping on saturated absorption spectra of thermal atomic vapor	77

4.1	Introduction	78
4.2	Theory and calculations	80
4.2.1	Reduced 5-level rate equation model	81
4.2.2	Reduced 7-level rate equation model	82
4.2.3	Atomic population relaxation	84
4.2.3.1	Spontaneous decay rate:	84
4.2.4	Calculation of absorption coefficient	85
4.3	Experimental setup	87
4.4	Results and discussion	88
4.4.1	5-level vs 7-level model for ^{87}Rb D ₂ line	88
4.4.2	Impact of pump saturation and magnetic sub-level pumping on resonances and crossovers	90
4.4.2.1	Resonances	90
4.4.2.2	Crossovers	92
4.4.3	Probe-induced hyperfine pumping	94
4.5	Conclusion	95
5	Optimization of Polarization Spectroscopy signal for laser-frequency stabilization	97
5.1	Introduction	98
5.2	Experimental method	100
5.3	Optical pumping induced birefringence	102
5.4	Results and discussion	105
5.4.1	Factors affecting Polarization Spectroscopy signal	106
5.4.1.1	Probe intensity	107
5.4.1.2	Pump intensity	108
5.4.1.3	Vapor cell temperature	109
5.4.1.4	Characterization of error signal for beam diameter $\sim 2 \times 1.67$ mm	111
5.5	Long-term frequency-stabilization of an ECDL using Polarization Spec- troscopy signal	113
5.6	Theory vs experiment	116
5.7	Conclusions	117
6	Conclusions and future outlook	121
6.1	Conclusion	121
6.2	Future outlook	124

Contents

Bibliography	127
List of Publications	139

List of Figures

1.1	Illustrations of the interactions between light and matter as depicted by three different theories — (a) semi-classical, in which the light field is represented as an oscillating electric field that follows the electric-dipole selection rules (see section 1.4.2) to excite atoms from one quantized atomic level to another; (b) fully quantum, in which atomic energy levels and light are both quantized; and (c) classical, in which an oscillating electric field displaces the center of the positive and negative atomic charge distribution, thereby inducing an oscillating dipole. By the Lorentz atom model, these oscillations are compared with the forced oscillation of a classical harmonic oscillator, such as a spring-mass system.	5
1.2	Schematic for the Einstein rate equation model for (a) two-level or closed system and (b) three-level or open system.	10

- 1.3 (a) Bohr atomic model for a single-valance electron in n^{th} shell having orbital angular momentum l and associated magnetic moment, μ_l , directing in the opposite directions. This model corresponds to the gross structure of the atom that includes only the kinetic energy and the Coulomb potential [7]. (b) The vector atom model shows the coupling between the total orbital (\mathbf{L}) and spin (\mathbf{S}) angular momentums, which precess about their resultant, i.e., total angular momentum vector ($\mathbf{J}=\mathbf{L}+\mathbf{S}$) of the electron(s). This L-S coupling perturbs the atomic Hamiltonian corresponding to the gross structure and splits the energy levels, characterized by \mathbf{L} -values, into the fine levels (each characterized by J-values) having energy shift $\Delta H_{LS} \propto \mathbf{L}\cdot\mathbf{S}$. (c) Further splitting of the fine energy levels into hyperfine levels results from the coupling between nuclear spin angular momentum (\mathbf{I}) and total angular momentum (\mathbf{J}) of the electron(s), which are represented by the vector atom model and precess around their resultant vector, $\mathbf{F}=\mathbf{I}+\mathbf{J}$, known as the hyperfine quantum number. The perturbation energy introduced in the fine structure Hamiltonian due to the I-J coupling is $\Delta H_{HFS} \propto \mathbf{I}\cdot\mathbf{J}$. (d) The energy level scheme for the gross, fine, and hyperfine structures corresponding to the alkali D-line (D₁-line: $n^2S_{1/2} \rightarrow n^2P_{1/2}$ and D₂-line: $n^2S_{1/2} \rightarrow n^2P_{3/2}$) transitions (having a single-valance electron with $\mathbf{S} = s = 1/2$ and $\mathbf{L} = l$). Here, the total number of $(2J + 1)$ fine levels is given by $J = |L - S|$ to $L + S$, and the total number of $(2F + 1)$ hyperfine levels is given by $F = |J - I|$ to $J + I$ 14
- 1.4 (a) Diagram illustrating that atomic levels with precise energy will result in a line spectrum; nevertheless, this experimentally observed spectrum has some linewidth that indicates that the energy levels are not precise but have some width (or uncertainty) due to the uncertainty in the time that atoms spend at that particular energy level. This line broadening is referred as the lifetime or natural broadening [1]. The schematic indicates that the excited state has a greater width than the ground state, according to the Heisenberg principle, because the lifetime of the ground state is substantially shorter than that of the excited state. (b) Illustration showing the ways that various atom velocity classes cause Doppler-broadening in a thermal atomic vapor. 20
- 1.5 Calculated Doppler-broadened transmission dips (solid lines) of the Rb D₂-line at vapor cell temperature 25 °C and length 75 mm using a 2-level χ -model [2]. The colored dotted and dashed curves for ⁸⁷Rb and ⁸⁵Rb, respectively, illustrate that each dip comprises three dipole-allowed hyperfine transitions $F_g \rightarrow F_e = F_g - 1$ (red), F_g (green) and $F_g + 1$ (blue). 26

2.1	(a) Hyperfine-level scheme and frequency separation for the Rb D_2 -line transitions for both isotopes (^{85}Rb and ^{87}Rb) and (b) schematic for the 5-level model indicating absorption in the presence of hyperfine pumping.	36
2.2	Experimental setup for studying the effect of variation of probe intensity, beam diameter and vapor cell temperature on the Doppler-broadened absorption spectrum of Rb D_2 -line.	45
2.3	Experimentally observed Doppler-broadened transmission spectra of Rb D_2 -line (coloured solid lines) show good agreement with the calculated transmission spectra using our 5-level model (black dashed line) at three different probe intensities ($0.01I_{sat0}$, $0.3I_{sat0}$ and I_{sat0}) with a fixed probe beam diameter ~ 2.86 mm and vapor cell temperature 24.2 °C. The black dotted line shows the spectrum calculated from the 2-level χ -model [2].	46
2.4	Calculated line-centre transmission vs normalized probe intensity I/I_{sat0} . The 5-level model (red solid lines) shows good agreement with experimental data (blue dots) for all 4 dips of the Rb D_2 line for beam diameter ~ 2.86 mm, and cell temperature 24.2 °C. The horizontal black solid line denotes the 2-level χ -model [2] which does not take probe intensity into account.	47
2.5	Normalized peak (i.e. line-centre) absorption coefficient α_{D0} vs normalized probe intensity I/I_{sat0} for three different beam diameters ~ 1.39 mm, 2.86 mm, 5.67 mm (with ellipticity $< 3\%$). The 5-level model (coloured solid lines) shows fairly good agreement with experimentally observed data (coloured dots) for (a) dip-iii and (b) dip-iv. The black solid line denotes the standard two-level model for a Doppler-broadened medium, i.e., $\frac{\alpha_{D0}(I)}{\alpha_{D0}(I \rightarrow 0)} = \frac{1}{\sqrt{1+I/I_{sat0}}}$. The exact values of the vapor cell temperature during these measurements are listed in table 2.2.	48
2.6	(a) Experimentally observed Doppler-broadened transmission spectra of Rb D_2 -line (coloured solid lines) with probe intensity $\sim 2I_{sat0}$, beam diameter ~ 2.86 mm at three different vapor cell temperatures: 24.2 °C, 36.5 °C and 53.5 °C show good agreement with the 5-level model (black dashed lines). (b) Normalized line-centre absorption coefficient α_{D0} vs normalized probe intensity I/I_{sat0} for dip-iv: 5-level model prediction (dashed black line) and experimental data (coloured dots) for vapor cell temperatures 24.2 °C, 36.5 °C and 53.5 °C at a beam diameter ~ 2.86 mm. The solid black line denotes the normalized line-centre absorption coefficient $\frac{1}{\sqrt{1+I/I_{sat0}}}$ for a 2-level system.	51

2.7	Comparison of 3-level and 5-level models with the experimentally observed normalized line-centre absorption coefficient for dip-iii of the Doppler-broadened transmission spectra of the Rb D ₂ line at beam diameter ~ 1.39 mm and vapor cell temperature 27.2 °C. It is evident that both models provide similar results for probe intensities $\lesssim I_{sat0}$. Beyond this, the result calculated from the 3-level model starts deviating from the 5-level model. Clearly, the 5-level model shows better agreement with the experimental data, supporting the argument given in [51].	53
3.1	(i) Hyperfine energy-level diagram for ⁸⁷ Rb D ₂ line. (ii) Schematic of the reduced 5-level scheme discussed in [59]. (iii-v) Zeeman pumping scheme for the ⁸⁷ Rb D ₂ line, including all the dipole-allowed Zeeman transitions present in the hyperfine transitions allowed from $F_g = 2$ to the excited states: $F_e = 1$ (iii), $F_e = 2$ (iv), and $F_e = 3$ (v) for σ^+ and σ^- polarizations. The effective line-strengths of the σ^+ and σ^- transitions, with corresponding weight factors of ‘sp’ and ‘sm’, respectively (see equation (3.1)) for an arbitrarily polarized probe, is mentioned at the top of each excited Zeeman level determined by their respective normalized dipole-matrix elements (see table 3.2). (vi) Schematic of the reduced 7-level model which groups the magnetic sub-levels lying in the ”bright” ($F_g = 2$) and ”dark” ($F'_g = 1$) hyperfine ground states, as well as in the excited state ($F_e = 1$ or 2 or 3) into the seven different atomic-levels to account for both Zeeman pumping and hyperfine pumping.	60
3.2	Experimental setup for studying the effect of variation of probe intensity and probe polarization on the Doppler-broadened absorption spectrum of Rb D ₂ -line.	69
3.3	For a \sim linearly ($\phi \sim 2^\circ$) and a right circularly or σ^+ ($\phi \sim 45^\circ$) polarized probes, calculated Doppler-broadened D ₂ line transmission spectra (solid lines) using our reduced 7-level rate equation model for the hyperfine transitions $F_g = 2 \rightarrow F_e = 1, 2, 3$ [(a) and (b)], and reduced 5-level rate equation model [59] for the hyperfine transitions $F_g = 1 \rightarrow F_e = 0, 1, 2$ [(c) and (d)] of ⁸⁷ Rb, show good agreement with the experimentally observed transmission spectra (colored dots). Here, the transmission spectra are measured at two different probe intensities, $\sim 0.02I_{sat0}$ and $\sim 0.3I_{sat0}$, with a fixed probe beam diameter ~ 3.04 mm and vapor cell temperature ~ 24 °C.	71

3.4	Comparison of the calculated (solid colored lines) line-center probe transmission vs normalized probe intensity I/I_{sat0} by using (a) 7-level rate equation model for the hyperfine transitions $F_g = 2 \rightarrow F_e = 1, 2, 3$, and (b) 5-level rate equation model for the hyperfine transitions $F_g = 1 \rightarrow F_e = 0, 1, 2$ of the ^{87}Rb D ₂ line with the experimental data (colored dots). Here, error bars represent the standard deviations of the mean line-center transmissions of the probe.	72
3.5	For a σ^+ pump, calculated atomic population fraction as a function of time in $ a\rangle$ (red curve), $ a'_p\rangle$ (green curve) and $ c\rangle$ (blue curve) for the dipole-allowed hyperfine transitions from $F_g = 2$ to (a) $F_e = 1$, (b) $F_e = 2$ and (c) $F_e = 3$ of the ^{87}Rb D ₂ line at two different probe strengths, $0.01I_{sat0}$ and $0.3I_{sat0}$	74
4.1	(i) Energy level scheme of the Rb D ₂ line. (ii) Magnetic Zeeman sub-levels incorporated into the reduced 7-level system corresponding to the hyperfine transitions $F_g = 1 \rightarrow F_e = 0, 1, 2$, and (iii) Schematic for the 5-level rate equation model that clubs together all the magnetic sub-levels within each hyperfine state.	80
4.2	Experimental setup for studying the saturated absorption spectrum of Rb D ₂ line under controlled pump and probe intensity, beam diameter, and vapor cell temperature.	88
4.3	Experimentally observed Doppler-free transmission spectra of the Rb D ₂ line (black solid lines) show good agreement with the calculated transmission spectra using our 5-level model (red dotted line) at probe intensity $\sim 0.01I_{sat0}$ and pump intensity $\sim 1.1I_{sat0}$ for beam diameter ~ 4 mm and vapor cell temperature ~ 25 °C.	89
4.4	(a-d) Zoomed-in view of all four transmission dips shown in figure 4.3. Our ab-initio reduced 5-level rate equation model (red dotted line) correctly predicts (with residual error $\lesssim 3\%$) all six SAS features, including three resonances ('L') and three crossovers ('X'), for dip i-iii (a-c). However, for dip-iv (d), this model doesn't capture the sign reversal at crossover X ₁₀ and slightly overestimates the transmission at crossover X ₂₁ , which is accurately predicted by our ab-initio 7-level rate equation model (blue dotted line) with residual error $\lesssim 3\%$	89

4.5	(i) Energy-level scheme for crossover X_{23} corresponding to transitions from ground state $ 1\rangle \rightarrow 2\rangle$ and $ 3\rangle$ and Doppler-shifts for the counter-propagating pump and probe for an atom with non-zero velocity, v_z , along the pump propagation direction. (iv, v) Magnetic sub-level pumping scheme for the crossover X_{31} , when a linearly polarized pump sees atoms with velocity $-v_z$ resonant to the lower hyperfine transitions $F_g = 2 \rightarrow F_e = 1$ (iv), and $+v_z$ resonant to the upper hyperfine transitions $F_g = 2 \rightarrow F_e = 3$ (v) (and vice-versa for the probe). Similarly, (vi, vii) magnetic sub-level pumping scheme for the crossover X_{10} , when a linearly polarized pump sees atoms with velocity $-v_z$ resonant to the lower hyperfine transitions $F_g = 1 \rightarrow F_e = 0$ (vi), and $+v_z$ resonant to the upper hyperfine transitions $F_g = 1 \rightarrow F_e = 1$ (vii) (and vice-versa for the probe). . . .	91
4.6	Comparisons between experimentally observed (black solid lines) ^{87}Rb D_2 line SAS spectra for different pump intensities ($I_{probe} \sim 0.01I_{sat0}$) with the calculated spectra using our reduced rate equation models. (a-c) The 5-level model (red dotted line), which includes hyperfine pumping but ignores Zeeman pumping, accurately predicts all of the SAS features with a residual error $\lesssim 3\%$ for dip i. However, for dip-iv (d-f), the 7-level model (blue dashed line), which accounts for the Zeeman (magnetic) sub-level pumping, is required to predict all the SAS features more accurately (residual error $\lesssim 3\%$) as compared to the 5-level model, especially, at crossovers X_{10} and X_{21} . Here, the beam diameter is ~ 4 mm and cell temperature ~ 25 °C.	92
4.7	Experimentally observed (a) dip-iv and (b) dip-iii of the Doppler-free Rb D_2 line transmission spectra, for linearly polarized probe ($I_{probe} \sim 0.1I_{sat0}$) and pump ($I \sim 7I_{sat0}$), show significant deviation from the calculated spectra using our 5-level (red dotted curve) and 7-level (blue dotted curve) models that do not incorporate the probe-induced hyperfine pumping (referred as 5-level ₀ and 7-level ₀ here). However, both models correctly predict the SAS spectra after including probe intensity in the pumping term of the rate equation (shown by green dashed lines in (a) and (b)), referred as 5-level _{0,1} and 7-level _{0,1} , respectively. These results are with pump-probe beam diameter ~ 2.86 mm at vapor cell temperature ~ 23.3 °C.	95
5.1	Experimental layout for Polarization Spectroscopy.	100
5.2	Zeeman level scheme of the strongest closed hyperfine transition $F_g = 2 \rightarrow F_e = 3$ (oscillator strength ~ 0.7) of ^{87}Rb D_2 -line in the absence of any external magnetic field, when (a) pump is off, the case in which all ground magnetic (m_g) sub-levels are degenerate and equi-populated; and (b) pump is on, the case in which σ^+ pump induces population anisotropy for D-polarized probe (combination of equal σ^\pm components) by pumping atoms to the extreme magnetic sub-level $m_g = +F_g$.	103

5.3	Doppler-broadened (black dotted line), and Doppler-free (red solid line) spectra corresponding to dips i and ii of the Doppler-broadened Rb D ₂ -line spectra, measured by a balanced photodiode at the (a) transmitted arm (PD _T), and (b) reflected arm (PD _R) of the PBS2. (c) Experimentally generated error or PS signal (PD _T – PD _R) for a D-polarized probe having intensity $\sim 0.3I_{sat0}$ in the presence of a σ^+ pump having intensity $\sim 2I_{sat0}$. Here the pump-probe beam diameter is ~ 1.67 mm, and vapor cell temperature is ~ 19 °C.	106
5.4	Experimentally observed PS (or error) signal corresponding to (a _i) dip-i and (a _{ii}) dip-ii of the Rb D ₂ -line for varying probe intensities (ranging from $\sim 0.05I_{sat0}$ – $\sim 1.5I_{sat0}$) at a fixed pump intensity $\sim I_{sat0}$. Variation of peak-to-peak value (b _i and b _{ii}) and slope (b _i and b _{ii}) of the most prominent error signals corresponding to the strongest Rb D ₂ -line hyperfine transitions ($F_g = 2 \rightarrow F_e = 3$ of ⁸⁷ Rb and $F_g = 3 \rightarrow F_e = 4$ of ⁸⁵ Rb, respectively) as a function of D-polarized probe intensity measured for three different σ^+ pump intensities, $\sim 0.5I_{sat0}$, I_{sat0} and $1.5I_{sat0}$, at a fixed pump-probe beam diameter ~ 1.67 mm and vapor cell temperature ~ 22 °C.	107
5.5	Experimentally observed PS (or error) signal corresponding to (a _i) dip-i and (a _{ii}) dip-ii of the Rb D ₂ -line for varying pump intensities (ranging from $\sim 0.05I_{sat0}$ – $\sim 10I_{sat0}$) at a fixed probe intensity $\sim 0.5I_{sat0}$. Variation of peak-to-peak value (b _i and b _{ii}) and slope (b _i and b _{ii}) of the most prominent error signals corresponding to the strongest Rb D ₂ -line hyperfine transitions ($F_g = 2 \rightarrow F_e = 3$ of ⁸⁷ Rb and $F_g = 3 \rightarrow F_e = 4$ of ⁸⁵ Rb, respectively) as a function of σ^+ pump intensity measured for three different D-polarized probe intensities, $\sim 0.5I_{sat0}$, $0.7I_{sat0}$ and $1.5I_{sat0}$, at a fixed beam diameter ~ 1.67 mm and vapor cell temperature ~ 22 °C.	108
5.6	Experimentally observed PS (or error) signal corresponding to (a _i) dip-i and (a _{ii}) dip-ii of the Rb D ₂ -line for varying vapor cell temperature (ranging from $\sim 19 - 45$ °C) at a fixed probe intensity $\sim 0.5I_{sat0}$ and pump intensity $\sim 2I_{sat0}$. Variation of peak-to-peak value (b _i and b _{ii}) and slope (b _i and b _{ii}) of the prominent error signals that correspond to the strongest D ₂ -line hyperfine transitions ($F_g = 2 \rightarrow F_e = 3$ of ⁸⁷ Rb and $F_g = 3 \rightarrow F_e = 4$ of ⁸⁵ Rb) as a function of vapor cell temperature measured at D- (or diagonally) polarized probe intensity $\sim 0.5I_{sat0}$, σ^+ pump intensity $\sim 2I_{sat0}$ and pump-probe beam diameter ~ 1.67 mm.	111

- 5.7 For the pump-probe beam diameter ~ 3.2 mm, the experimentally observed peak-to-peak value (a_i) [and a_{ii}] and slope (b_i) [and (b_{ii})] as a function of pump intensity, varying from $\sim 0.05 - \sim 5I_{sat0}$, measured at probe intensity $\sim 0.3I_{sat0}$ and vapor cell temperature ~ 20 °C; and peak-to-peak value (A_i) [and (A_{ii})] and slope (B_i) [and (B_{ii})] as a function of vapor cell temperature, varying from $\sim 17 - 42$ °C, measured at probe intensity $\sim 0.3I_{sat0}$, and pump intensity $\sim I_{sat0}$ for the error signals corresponding to the strongest D₂-line hyperfine transition $F_g = 2 \rightarrow F_e = 3$ of ⁸⁷Rb [and $F_g = 3 \rightarrow F_e = 4$ of ⁸⁵Rb]. Here, the probe is D-polarized and the pump is σ^+ polarized. 112
- 5.8 Schematic of laser frequency locking mechanism (leftmost box) and the experimental setup for locking the ECDL frequency using PS signal. 114
- 5.9 Wavelength vs measurement time, when the laser is (a) unlocked and locked utilizing the prominent PS signals corresponding to the closed Rb D₂-line transitions (i) $F_g = 2 \rightarrow F_e = 3$ of ⁸⁷Rb [**dip-i**] and (I) $F_g = 3 \rightarrow F_e = 4$ of ⁸⁷Rb [**dip-ii**]. The ECDL's wavelength distribution & its measured linewidth over the time-period of ~ 60 mins demonstrate the rms drift in the central frequency of the laser is reduced to ~ 450 kHz (ii & iii) [and ~ 400 kHz (II & III)], when it locked using the strongest error signal corresponding to **dip-i** [and **dip-ii**], as compared to the rms drift ~ 9 MHz corresponding to the unstabilized laser (a and c). 115
- 5.10 Comparison of the experimentally observed (red dots) and calculated PS signal (black solid line) corresponding to $F_g = 2 \rightarrow F_e = 1, 2, 3$ of the ⁸⁷Rb D₂-line (dip-i) using a full multi-level rate equation model (black line) [39, 43] at pump intensities (a) $\sim I_{sat0}$ and (b) $\sim 10I_{sat0}$. A qualitative comparison between the theoretically calculated (black solid line) and experimentally measured (c) peak-to-peak amplitude (red dots) and (d) slope (blue dots) of the strongest PS signal, which corresponds to the closed hyperfine transition $F_g = 2 \rightarrow F_e = 3$ of ⁸⁷Rb D₂-line, utilizing the analytical model discussed in [86]. Here, the probe intensity is $\sim 0.3I_{sat0}$ and pump-probe beam diameter is ~ 1.67 mm. 116

List of Tables

2.1	The relative coupling strength of the three dipole-allowed hyperfine transitions from the upper hyperfine ground state of (a) ^{87}Rb , and (b) ^{85}Rb ; and lower hyperfine ground state of (c) ^{85}Rb , and (d) ^{87}Rb (corresponding to dips (i-iv) of the transmission spectrum respectively, see figure 2.3) [5, 18, 19]:	41
2.2	The experimental data for absorption saturation for three different beam diameters shown in figure 2.5 are fitted to the function $\frac{1}{\sqrt{1+\beta\frac{I}{I_{sat0}}}}$. Here, $\beta = \frac{I_{sat0}}{I_{sat}}$ is a parameter which gives the factor by which the saturation intensity is lowered (due to hyperfine pumping) as compared to the ideal 2-level system.	49
2.3	β (factor by which the saturation intensity is lowered due to hyperfine pumping, as defined in table 2.2) for dip-iv at seven different $1/e^2$ beam diameters. The corresponding values of atomic transit time ($\sim 1/\Gamma_t$) are also listed in order to compare with the typical time-scale of optical pumping ($\sim 10 \mu\text{s}$, for $I \sim 0.1I_{sat0}$) [38, 43]:	49
3.1	The Clebsch-Gordan coefficient of the dipole-allowed D_2 line hyperfine transitions from the (a) upper and (b) lower hyperfine ground state of ^{87}Rb respectively [2, 5, 15, 18, 19]	66
3.2	The effective coupling strength for the dipole-allowed σ^\pm ($\Delta m_F = \pm 1$) transitions in the hyperfine transitions $F_g = 2 \rightarrow F_e = 1, 2, 3$ (see figure 3.2) is $S_{F_g, m_{F_g} \rightarrow F_e, m_{F_g} \pm 1} = \frac{d_{F_g, m_{F_g} \rightarrow F_e, m_{F_g} \pm 1}^2}{\sum_{m_{F_g}=F_g-1}^{F_g+1} d_{F_g, m_{F_g} \rightarrow F_e, m_{F_g} \pm 1}^2} \times \text{weight factor}$ (i.e. sp and sm, respectively). Here, the first term in this product is the normalized value of the square of the electric-dipole matrix element [18].	67
5.1	The optimal region/value of the pump intensity and vapor cell temperature determined for two different beam diameters, where the error signal corresponding to the hyperfine transitions (a) $F_g = 2 \rightarrow F_e = 3$ of ^{87}Rb (dip-i), and (b) $F_g = 3 \rightarrow F_e = 4$ of ^{85}Rb (dip-ii) are more robust to any fluctuation that arises in these external parameters are listed below:	113

Abbreviations

NIR	Near-infrared
EM	Electromagnetic
FWHM	Full Width at Half Maximum
SAS	Saturated Absorption Spectroscopy
PS	Polarization Spectroscopy
EIT	Electromagnetically Induced Transparency
EIA	Electromagnetically Induced Absorption
ECDL	External Cavity Diode Laser
HWP	Half Wave Plate
QWP	Quarter Wave Plate
PBS	Polarizing Beam Splitter
PD	Photo-Diode
ND	Neutral Density
AOM	Acousto-Optic Modulator
EOM	Electro-Optic Modulator
DAVLL	Dichroic Atomic Vapor Laser Locking
PDH	Pound-Drever-Hall
GUI	Graphical User Interface
PID	Proportional-Integral-Derivative Analysis
PZT	Piezo-Electric Transducer

Symbols

c	speed of light in vacuum
Γ	natural linewidth
k	wavevector in free space
ω	angular frequency
ω_{e_2, e_1}	angular frequency separation between excited states e_2 , and e_1
λ	wavelength
\hbar	reduced Planck's constant
l	orbital angular momentum in units of $2\pi\hbar$
I_{sat0}	2-level saturation intensity
n_i	atomic population in the i^{th} atomic state
F	hyperfine quantum number
m_F	hyperfine magnetic quantum number
B	Einstein B coefficient